HiSST: 3rd International Conference on
High-Speed Vehicle Science Technology
14 -19 April 2024, Busan, Korea

Development of Neuromorphic Imaging Spectroscopy for Hypersonic Flight Observation

Tamara Sopek[1], Fabian Zander[2], Byrenn Birch[3], David Buttsworth[4]

Abstract

Enhanced capability to collect vital hypersonic flight data is required to better understand the physics of the flow around spacecraft entering Earth's atmosphere. Using novel, bio-inspired cameras will allow spectral measurements to be performed equally well during the day and night without modifications to instrumentation, overcoming the current major limitation of daytime tests. Combining these cameras with high resolution spectroscopy enables more reliable collection of critical data, such as temperature and species composition from the flow around spacecraft on re-entry. Measurements were performed using a novel neuromorphic spectroscopy system and a range of light sources. Acquired data show that both broadband and line spectra were obtained. The present work demonstrates, for the first time, that a spectroscopy system set up based around neuromorphic technology is capable of measuring emission spectra. These results present a landmark first step in developing advanced spectroscopy diagnostics for hypersonic flight observation, such as observations of Earth re-entry missions.

Keywords: *hypersonic, optical diagnostics, spectroscopy, radiation*

Nomenclature

Latin
EB – Event-Based
L – luminance, cd/m^2
SNR – Signal to Noise Ratio

Greek
α – Tilt angle, °
Δ – difference

1. Introduction

The coming 20 years will see the next space race, but this time we are going to other planets, in particular Mars. For example, the USA is striving to achieve a Mars human space flight mission by 2033 [1]. A human-crewed mission to Mars will vary considerably from previous robotic missions. Compared to past robotic exploration campaigns to Mars, a human mission infers a return trip, further amplifying the technological difficulty. For example, despite concerted research efforts and progress, there still exist considerable uncertainties associated with the modelling of heat loads on the heat shield of the re-entry vehicle. During a conventional Earth atmospheric re-entry from deep space, such as a Mars return mission, the spacecraft will experience velocities higher than any Earth re-entry vehicle has experienced before. The spacecraft velocities will potentially exceed 14 km/s - substantially faster than Space Shuttle's re-entry from Low Earth Orbit (7.5 km/s), or the Apollo Lunar return missions (11 km/s). This will result in immense radiative and convective heating during re-entry and deceleration, and if the heat shield were to be based on the current technology, its mass would become unacceptably high. In a robotic mission, high heat shield mass directly translates to a low payload mass fraction; in a human mission, it results in less crew members. Significant improvements in the modelling of heat transfer to the heat shield are required to reduce the heat shield's mass, enable an improved and safer space vehicle design with higher payload mass fraction, and make such a mission feasible. Additionally,

[1] *University of Southern Queensland, Toowoomba Queensland 4350, tamara.sopek@unisq.edu.au*
[2] *University of Southern Queensland, Toowoomba Queensland 4350, fabian.zander@unisq.edu.au*
[3] *University of Southern Queensland, Toowoomba Queensland 4350, byrenn.birch@unisq.edu.au*
[4] *University of Southern Queensland, Toowoomba Queensland 4350, david.buttsworth@unisq.edu.au*

Copyright © 2024 by author(s)

research in rocketry is currently on the uptick internationally. Worldwide, companies such as SpaceX and Rocket Lab are investing enormous efforts and funds on concepts such as re-usable rockets and planetary exploration systems. Starship and Neutron are examples of such reusable transportation systems which can carry both crew and cargo to Earth orbit, the Moon, Mars and beyond.

Thus, there is a strong incentive to better characterise thermal conditions experienced during hypersonic flight. Ultimately, this will result in advancing the spacecraft design required to make human interplanetary flight possible. The proposed sensor will allow for enhanced collection of radiation spectroscopic data during both day and night hours, thus offering a dramatic capability increase for terrestrial optical sensors. Analysis of the acquired data will provide heat shield temperature and species composition information which will be used for the development of theoretical models (of re-entry aerothermodynamics, disintegration of spacecraft/meteors, etc.) and augmentation of existing databases, and also for benchmarking ground-based experiments and numerical simulations.

1.1. Experimental environment

The only two options for generating realistic aerothermodynamic conditions for studying these phenomena are high-speed ground test facilities, or flight experiments. However, although the ground test facilities [2] are capable of replicating aspects of high-speed flows, it is not possible to fully replicate the real flight environment. The only way this is possible is through flight testing, which can be expensive. Thus, researchers conduct remote observations of high-speed flight events to obtain the best possible radiation data. Since the opportunity to take measurements of hypersonic flight is rare, there is a drive to maximize the collection of highly valuable data from every such event.

1.2. Diagnostics

The common approach to remote observations is to use a combination of a scientific camera and a grism/grating to acquire spectroscopic data [3] providing additional information on the observation target. In ground-based observations, a large drawback is a considerable amount of atmospheric absorption of radiation. Also, while standard cameras can record objects appearing on a clear blue sky, this is difficult and demands some compromises due to saturation and noise in this environment. Additionally, many of the relevant events occur over the ocean which eliminates the possibility of ground-based observations. While the issue of atmospheric absorption and flights over the ocean can be tackled with airborne observations which remove the concern of clouds and accessibility, the problem of background brightness remains. Therefore, due to current technology limitations with remote observation of spacecraft entering the Earth's atmosphere, highly valuable spectroscopic measurement data is scarce. Neuromorphic EB vision is a novel technology with advantages in sensor performance when compared to conventional cameras, as illustrated in Fig.1. Measurements with this technology can be performed equally well during both day and night without modifications to instrumentation. The coupling of this neuromorphic camera with a spectrometer for neuromorphic imaging spectroscopy has never been trialed and is thus novel.

This study is motivated by the need to advance critical airborne remote diagnostics of hypersonic/space flight and the results presented here demonstrate a first step and essential contribution to development of such capabilities. This paper reports efforts to contribute towards development of a state-of-the-art optical spectroscopy technique that would allow for a more flexible, cost-efficient and responsive diagnostics for collection of invaluable hypersonic/space flight data through remote observations. The expected outcome is a new method which (1) allows acquiring of extremely rare and valuable information about the flow field of hypervelocity flight vehicles (such as temperature and species composition), at a higher fidelity than is possible with the currently available technology, and (2) enables measurements to be taken during daytime (a capability which is extremely difficult with standard cameras). To this aim, radiation measurements were performed with the goal of producing a set of benchmark data using a neuromorphic spectroscopy system. Newly developed neuromorphic spectroscopy system was used to monitor the radiation from a range of light sources over the spectral range of 400-900 nm, the sensitivity band of the cameras presently available to the authors.

Copyright © 2024 by author(s)

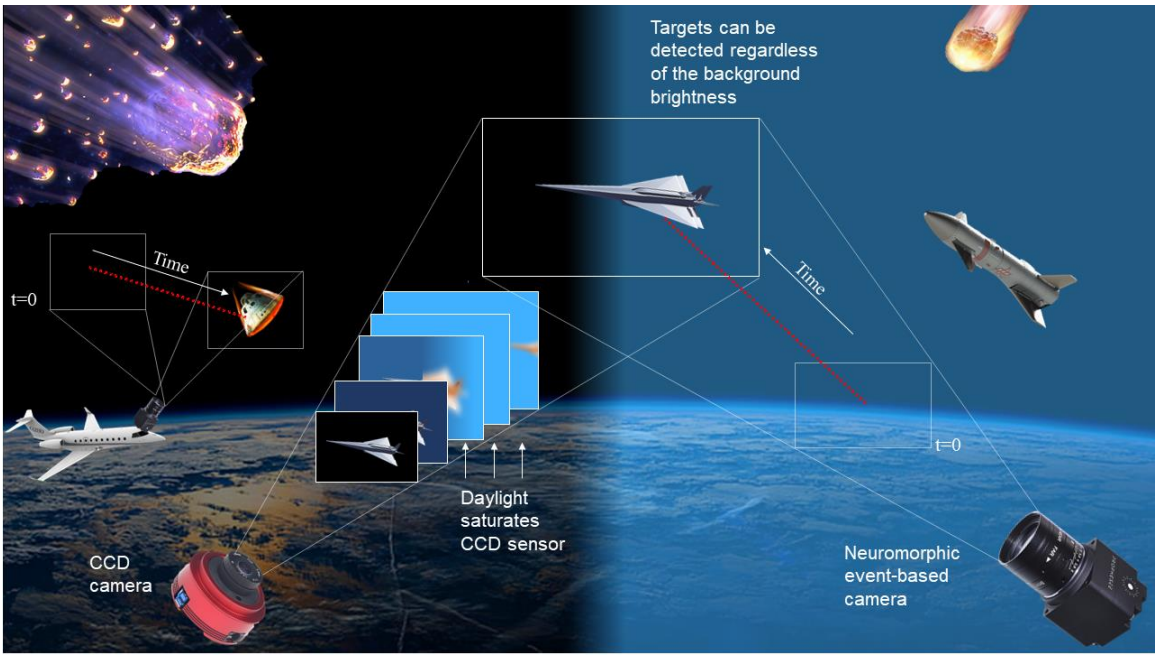

Fig. 1 Event-based space imaging compared to the standard CCD sensor approach. Adapted from Afshar [4].

2. Event-based cameras

Currently, capturing the spectral data of objects with the sky-background during daytime is extremely challenging - an object appearing in the sparsely populated field such as clear blue sky might not appear on the image due to low signal-to-noise ratio. This presents a major obstacle in performing both ground-based and airborne observations of events such as spacecraft re-entry or rocket launch as only certain geographical locations and/or hours are suitable, thus limiting the amount of scientific data to be collected in these events which are already limited by their low frequency of occurrence. Also, there are only a handful of research groups across the world performing observation of hypersonic flight events [5,6,7] which further limits the probability of obtaining high quality data, which directly affects the progress of science based on those measurements.

EB cameras are novel dynamic vision devices based on human retina that present "a paradigm shift in the way visual information is acquired" [8]. Usually known as neuromorphic imagers, these cameras record only when there is a light intensity change in the field of view. This means that instead of measuring the "absolute" brightness all the time, they respond to brightness changes in the scene asynchronously and independently for every pixel. They present a new and emerging hardware capability, and due to their advanced method of data collection, have recently been successfully used for a myriad of applications, from robotics to object/gesture recognition to particle velocimetry [8]. The most relevant application for this work is their use for star tracking and mapping [9] - because they don't continually record data, the problem of vast amounts of data created when imaging empty space is avoided. Also, as they only detect logarithmic light intensity changes, they can cover a wide range of illumination levels. Thus, the detection and recording of targets is enabled regardless of the background brightness, and imaging is performed equally well during day and night without modification of the sensors.

2.1 Principle of operation of event-based cameras

While traditional camera outputs frames at fixed time intervals, an EB camera outputs visual information about the scene as asynchronous events at microsecond resolution and transmits data with sub-millisecond latency. An event is generated each time a single pixel detects a light intensity change in the FOV — when a given pixel's luminosity change reaches a given threshold, it produces a visual event with an x and y address, a timestamp, and a polarity, which is either "ON" or "OFF" depending on the change in relative luminosity. Thus, the output of an EB camera is a stream of digital "events" or

Copyright © 2024 by author(s)

"spikes" of variable speed, with each event corresponding to a pixel's preset level of change in log intensity at a particular time. In mathematical notation, the output of an EB camera is a stream of N events e_i expressed as:

$$e_i = [x_i, y_i, t_i, p_i]_{i=1,\ldots,N}$$

where x, y are the spatial coordinates in units of pixels, t is the timestamp of the event, and $p \in \{-1,1\}$ is the polarity of the event (the sign of the log intensity change). This visual information encoding is inspired by the spiking nature of biological visual/optic pathways and the address-event representation (AER) [10] is commonly used in neuromorphic engineering. After the information is transmitted from the sensor, each pixel memorises their last log intensity and continuously monitors for a change of predefined magnitude from this memorised value. Once that change has been observed and recorded, the sensor sends another event. This change or contrast threshold can be written as:

$$\pm C = \log I\,(u,t) - \log\, I(u, t - \Delta t)$$

where C is contrast sensitivity (typically 10–15% of the relative brightness change), $\log(I)$ is the logarithmic change of light intensity, $u = \{x, y\}$, t is the timestamp of the event and Δt is the time since the previous event at the same pixel. The logarithmic relationship represents pixels' response to percentage changes in illumination rather than the absolute magnitude of the change, resulting in pixels operating over a very wide dynamic range. The EB cameras transmit events from the pixel array to periphery and subsequently out of the camera using a shared digital readout pipeline. When multiple new events are detected while a previous event is being transmitted, they are treated as simultaneous. These simultaneous events are transferred in an order determined by an arbiter system, and because they are timestamped during readout, they may not share the same timestamp. An arbiter ensures that pixel events are queued and wait their turn to access the shared readout pipeline, and that a row or column that is managed by the arbiter is guaranteed not to be dealt with again before all other rows and columns that have registered event detection have been managed.

Asynchronous EB pixel arrays are based on the idea that significant amount of the information conveyed by an event is in its precise timing of occurrence, particularly important in use of EB cameras in high-speed applications like high-speed tracking and optical flow with kHz update rates. Thus, event early-timestamping is imperative, i.e., as early as possible in the signal processing chain, to avoid any effects from the readout process on the timing of the event. EB camera used here has typical latency for a single event readout from pixel firing to the timestamp of around 60-70 ns, and pixel latency (delay between the light intensity change in the scene and the contrast detection by the pixel) of 200 μs, while timestamp precision is 1 μs.

The AER communication circuits losslessly transmit all events, however, the readout pipeline can become saturated, affecting the times that events are sent. In some high activity scene conditions, as the event detection rate increases, the limitations of readout are reached, and the event detection rate becomes higher than the maximum readout speed. This causes the simultaneous events queueing to be transferred to accumulate, resulting in an increased readout latency and introducing a timestamp error. The EB cameras have readout rates ranging from 2 MHz [11] to 1200 MHz [12], depending on the sensor and type of hardware interface. In most applications, the latest series EB camera readout systems can handle sustained rates of at least 100-200 MHz without much impact on timestamp accuracy. The timing of events can be reported with a very accurate temporal resolution in the order of microseconds and visual information is no longer acquired based on, for example, global shutter, but each pixel has its own sampling rate. Therefore, these sensors capture visual information predominantly in the time domain, contrary to the traditional frame-based cameras which provide greater amount of spatial information. Because the EB camera pixels only detect temporal changes, time-constant information such as static background is not captured. Since this information is redundant anyway, result is a sparser representation of the scene than with standard cameras, translated into EB cameras having higher temporal resolution with a very low data rate.

While EB cameras do not output images, it is possible to create pseudo images by integrating events stream for a chosen length of time. Fig.2 shows the example of EB camera output with and without light intensity change, created by integrating a stream of events for Δt=33 ms.

The advantages of neuromorphic EB imaging include high dynamic range, high temporal resolution, no motion blur, low mass, low latency and low power consumption, reduced bandwidth, as well as

Copyright © 2024 by author(s)

significant reductions in data storage requirements. EB neuromorphic cameras provide capabilities that cannot be achieved using conventional scientific cameras and thus present a game-change in remote observations. These cameras emit data as a spatio-temporal pattern rather than using conventional frames. The sensor pixels are independent and asynchronous, and there are no fixed exposure times, which results in high temporal resolution and high dynamics range of the device. These sensors can continuously image during motion, allowing the camera to move arbitrarily whilst still capturing valid data which is ideal for low stability environments such as airborne observations. Thus, they can capture the object in focus and the background objects without generating streaks generally found when imaging events such as a capsule re-entry or meteor shower. The high dynamic range allows that the same sensor can perform equally well during the day and nighttime without modifications in the instrument configuration. While a typical scientific camera based on charged-coupled-device (CCD) sensor produces frames of pixel intensities, an EB sensor generates a continuous stream of events. Each event is generated only in response to changes in the light intensity of an individual pixel. Due to this sparse spatio-temporal output, the data obtained with these devices must be interpreted in a substantially different way to traditional imagers.

Fig. 2 Example of an event-based camera output with a) no motion and b) with motion in the scene. In b), ON and OFF events are captured where ON is increase and OFF is decrease in logarithmic light intensity. Event stream integrated for Δt=33 ms.

Thus, the disadvantages of EB imaging include the inability to use traditional vision or image processing algorithms because of asynchronous pixels and no light intensity information (only binary intensity changes). New methods are required to rethink the spatio-temporal, photometric and stochastic nature of event data. Intensity calibration presents a significant challenge and has not been attempted yet according to the authors' knowledge. In case when there is no change in light intensity, such as a static scene, there is no creation of events and thus the only output is background noise. EB cameras' asynchronous event readout scheme has a limited maximum readout speed, which can become an issue in extremely active scenes. Additionally, as these cameras are not a mature technology, there is a limited number of manufacturers (including currently available resolution) and a limited base of knowledge. Table 1 provides a comparison between an event-based and a standard camera. The latter is not the best available but a typically used camera is authors' work on hypersonic flight observations.

Table 1 Comparison of an EB and a standard camera typically used in authors' work.

	Event-based camera (Prophesee Gen4)	**Standard camera (QHY5III174)**
dynamic range	high (>120 dB)	low (75.6 dB)
max fps (update rate)	high (asynchronous): >10kfps	low (synchronous): 138 fps
resolution at max fps	> Mpxl	> Mpxl
data rate	≈1 GB/s	5 GB/s
bits per event/pixel	≈40 bits/event	12 bits/pixel
weight	40 g	89 g
resolution	1280 x 720 px	1936 x 1216 px

Copyright © 2024 by author(s)

pixel size	4.86 μm	5.86 μm
motion blur	no	yes
absolute intensity	no	yes

The success achieved in using these cameras for Space Situational Awareness (SSA) [10] provides confidence in their successful application for the different type of space imaging proposed here. The aim of this project is to develop an optical sensor based on a combination of an EB camera and a grism (grating + prism) slitless spectrometer for remote sensing of radiation. We are the first to couple this neuromorphic imager with a slitless spectrometer.

3. Experimental Setup

The event-based camera is paired with a slitless spectrometer to enable collection of spectroscopic data. The slitless spectrometer is a well-known and commonly-used method to capture spectral emissions of phenomena such as shock layer radiation of a sample return capsule [6-8] or space debris [5]. It typically consists of an order-sorting prism, transmission grating, lens and possibly a filter. The prism refraction angle is typically chosen to redirect the centre wavelength of the observed spectrum back onto the optical axis. However, the spectrometer design in this study was simplified by tilting the recording end of the system at a tilt angle α, as shown by example in Fig.3. This removes the need for a prism, which enables us to keep the image of the spectrum parallel to the focal plane, as well as maintaining focus on all colours of the spectrum.

Experiments reported in this study were performed using a Prophesee Gen4 EB camera with embedded Metavision® IMX636 sensor, camera lens, transmission grating, filter and a light source. Two variations of spectrally resolved measurements were performed for this study, using a:

- integrating sphere
- mercury/argon lamp

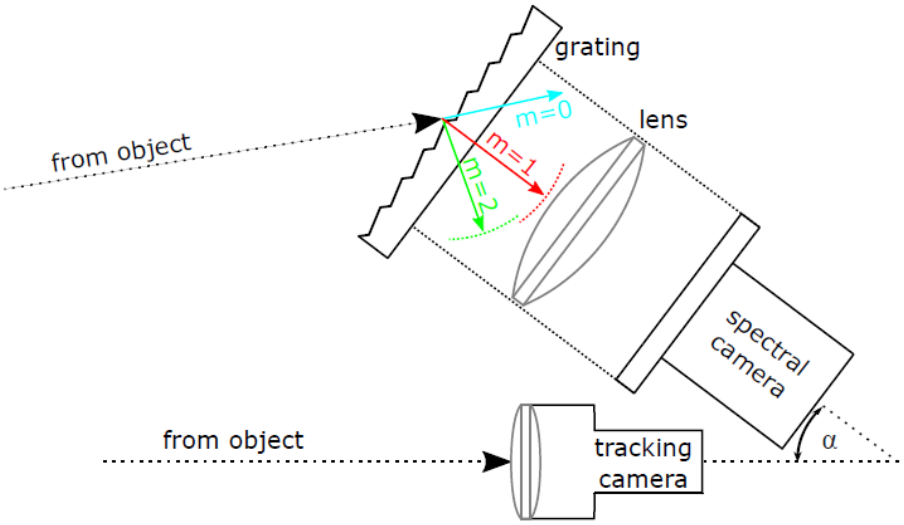

Fig. 3 Example of a slitless grating spectrometer. Adapted from [6].

5.1 Optical Instrumentation

The optical arrangement during these experiments was designed to enable the recording of the spectrally and spatially resolved radiation emitted from several different light sources. These radiation experiments employed an optical emission spectroscopy (OES) system covering the spectral range of approximately 400-900 nm.

Accurate calibration of the recorded data is a vital part of the process for all experimental measurements. All elements on the optical path, such as windows, gratings and filters, are associated

Copyright © 2024 by author(s)

with a specific wavelength-dependent efficiency with which they transmit light. Calibration of all spectral data needs to be done to convert the EB camera output into standard light intensity units. However, this is not a small task by any means - since EB cameras operate in such a way that only the logarithmic light intensity changes are recorded and not the absolute intensity, these systems need to be calibrated for the conversion of recorded data into absolute intensity. As explained earlier, the output of EB camera systems, besides pixel address and timestamp, includes only binary light intensity change information instead of counts like in standard camera frames. Though those frames also need calibration with a known output light source to convert output into standard units, the process is straightforward. In EB systems, as there is only binary information of the luminance change and not the quantity value, the calibration process is infinitely more challenging, and to our knowledge, has never been attempted before. This part of the project is currently under way and results will be reported in another publication.

4. Results and Analysis

4.1. Spectral calibration

4.1.1. Spectral calibration using a broadband light source

Radiation intensity measurements were performed using a broadband light source Labsphere PT-038-PLS. This is a tunable LED light source which was used with a 5 mm diameter port, while the output luminance was set to 500 cd/m^2. Reported results in Fig.4 were obtained using Δt=33 ms to create a pseudo image from the events stream. Table 2 provides details on spectrometer properties for both EB and standard camera systems. While EB camera does not output images, it is possible to create pseudo images by integrating events stream for a chosen length of time. For majority of pseudo images presented in this work, the integration time was chosen to equal the standard camera exposure time of Δt=33 ms. However, to show the full capabilities of EB camera dynamic range, the integration time was changed, and this is described in Section 4.2.

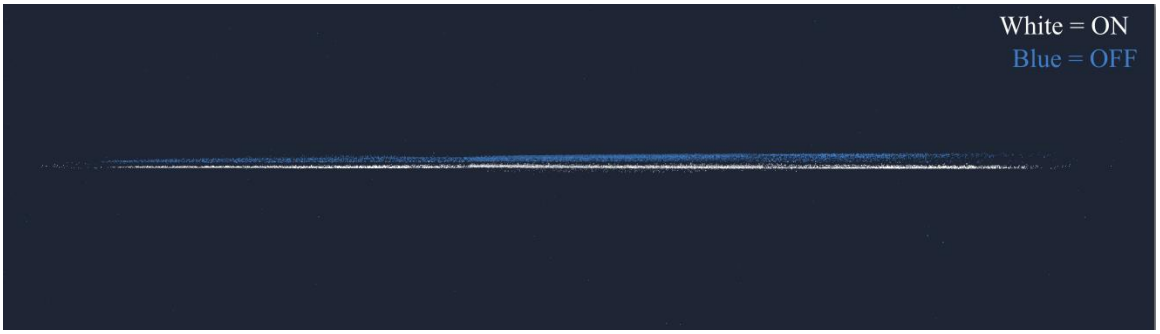

a)

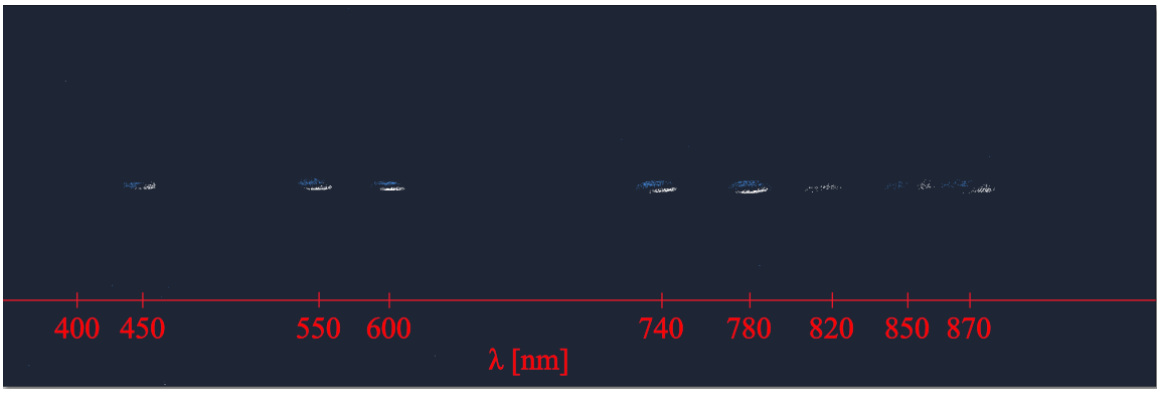

b)

Fig. 4 Example of spectra from a broadband light source: a) broadband spectrum and b) sections of broadband spectrum obtained with bandpass filters (FWHM=10 nm).

Copyright © 2024 by author(s)

Table 2 Summary of the spectrometer properties.

Instrument	THUNDER	ASTRO
sensitivity band [nm]	350-900	350-900
resolution [px nm^{-1}]	2.8	7.12
spectral width [nm]	440	270
horizontal field of view [°]	22	12.8
grating blaze angle [°]	29.87	29.87
grating [lines/mm]	830	830
camera	Prophesee Gen4	QHY5III174
sensor	Sony IMX636HD	Sony IMX174
pixel array	1280 x 720	1936 x 1216
pixel size [μm]	4.86	5.86
integration time [s]	0.033 (pseudo images)	0.033

4.1.2. Spectral calibration using a spectral line light source

This set of measurements was performed using a Mercury-Argon spectral calibration source. Data was collected through emission spectroscopy technique as in previous section. This is an Avantes AvaLight-CAL-HgAr calibration source with output in the 253.6-922.5 nm spectral range. The optical power in 600 µm fiber is 1.6 mW. Results obtained with this light source are shown in Fig.5. Result shown in Fig.5a was obtained using Δt=33 ms to create a pseudo image from events stream. Fig.5b illustrates spectral line output from the calibration source as reported from the manufacturer. This was used for wavelength calibration of the EB camera recordings, i.e., to identify specific spectral lines. The same calibration light source output was then recorded with a compact spectrometer, a Thorlabs CCS175 Czerny-Turner spectrometer for wavelengths ranging from 500-1000 nm that was connected with a fiber optic cable to the light source to capture the emitted radiation. The result is shown in Fig.5c.

4.2. Dynamic range

To demonstrate the extended dynamic range of the EB camera in a spectroscopy setup, the EB and standard camera spectrometers were mounted side-by-side and recorded output of the broadband light source (Labsphere PT-038-PLS) at varying luminance levels. These measurements were done in a dark room. Standard camera spectrometer used settings we typically employ in airborne observation missions when we are recording radiation from a spacecraft re-entering the Earth's atmosphere. The EB camera had some settings adjusted for noise removal and low light (i.e., increase sensitivity of the sensor to detect positive changes in the light intensity), while other settings were left at default values of the Metavision® SDK version 4.5.1. The integration time for pseudo images was reduced to Δt=10 μs. This time interval was chosen as it corresponds to the average time it takes from when a row of a pixel firing is readout for the first time to the time when the same (or close-by) row of pixel firing is readout again. The settings for both spectrometers are listed in Table 3.

Table 3 Summary of the camera recording properties.

Instrument	THUNDER	ASTRO
integration time [s]	$10e^{-6}$ (pseudo images)	0.033
fps	1M	30
gain	-	480
bias fo	55	-

Copyright © 2024 by author(s)

bias hpf	60	-
bias diff_on	-30	-

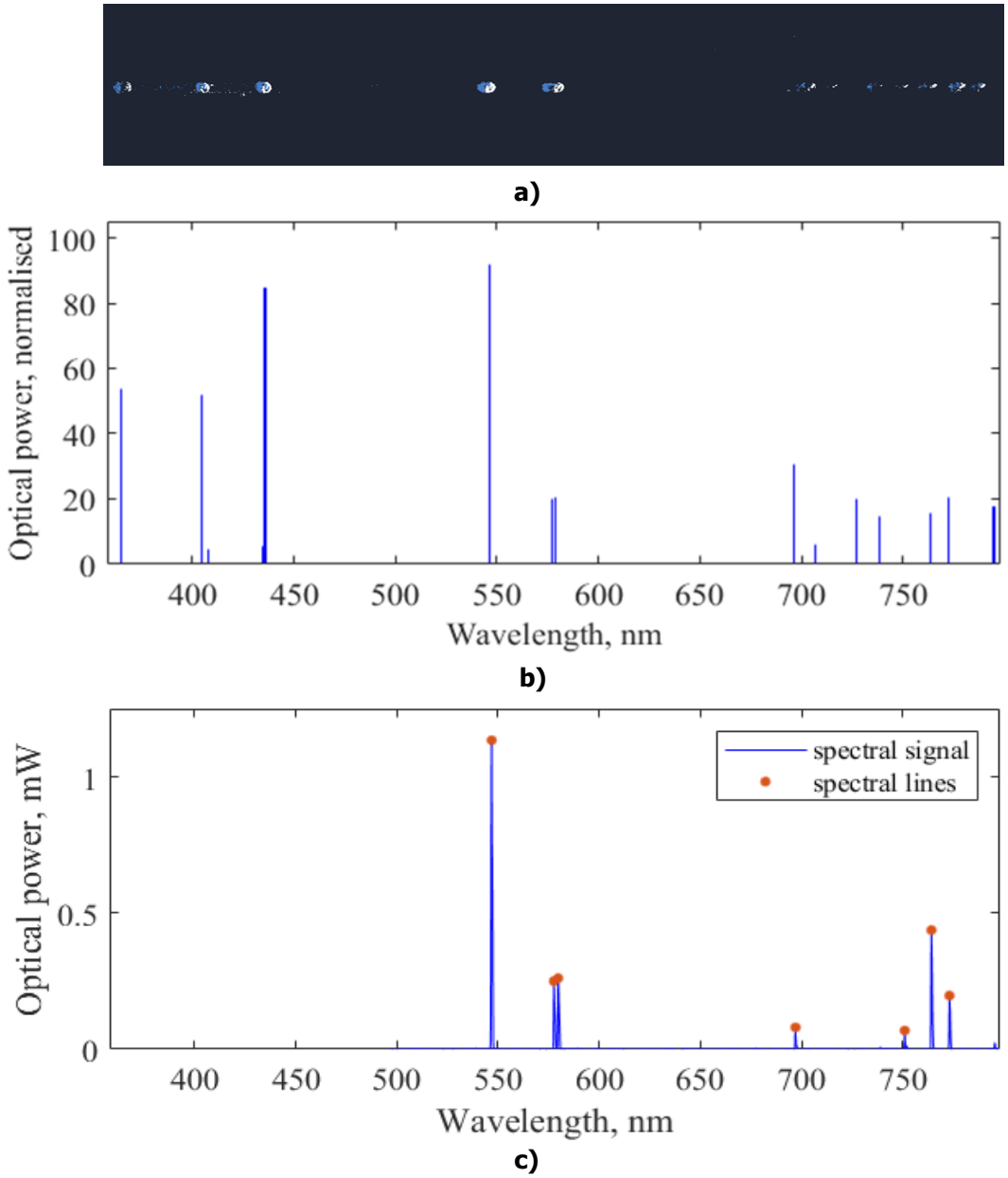

Fig. 5 Example of spectra using a spectral line light source: a) line spectra recorded with EB camera, b) calibration source output and c) line spectra recorded with a compact spectrometer.

Since the EB camera records only when there is a change of light intensity on the field of view, an iris was used to block the light source prior to recording and once the recording started, the iris was opened to let the light in. A motorized iris was used for precise and quick control of the aperture. The methodology was as follows:

- Luminance output of the light source was varied, initially in increments of 1 cd/m^2 and measurements taken with both systems.

Copyright © 2024 by author(s)

- Images from the standard camera were inspected to determine whether the broadband spectrum is visible in the image. Pseudo images from the EB camera were inspected as well, and full line of broadband spectrum was targeted.
- If the spectrum in both systems was not detected, the luminance was increased. When the spectrum was detected, the related luminance level was set as the lower bound for that system.
- The luminance was increased further, in larger increments of 10 cd/m^2. Once the inspection of images from the standard camera system confirmed that the image was over-exposed, the previous luminance level was taken as the upper bound for that system. The luminance was increased further for the EB system. As the EB cameras don't have standard images or exposure, there is no over-exposure either.

The results of this process are shown in Fig.6. Images from both systems are shown at particular luminance levels. The EB camera shows a partial spectrum already at the starting luminance level of 1 cd/m^2, however it is not a full spectrum and thus was not deemed satisfactory. Standard camera images also show spectrum at the lowest luminance setting; however, the signal-to-noise ratio (SNR) is too low for these to be useful. The luminance level of 5 cd/m^2 was determined to be the lower bound for both the EB and the standard camera system. Images show full spectra at good enough SNR to be able to extract information. The upper bound of the standard camera system is at 80 cd/m^2. The one of the EB camera system is more difficult to determine at the moment as the intensity calibration has not been completed. However, we determined this to be at approximately 500 cd/m^2, as the shape of the spectrum starts to change slightly. At this luminance, the spectrum obtained with the EB system shows a small bump on the upper side. These results show that while both systems seem to have the same lower bound, the standard camera system's upper bound is already at 80 cd/m^2, while the one of the EB system is much higher at 500 cd/m^2. This large difference illustrates the extended dynamic range of the EB camera in the spectroscopy setting. This is particularly relevant in daylight applications, where the standard cameras easily get overexposed. It is important to note, however, that the reported values are used here for comparative purposes only, as luminance is a photometric quantity which would need to be converted to its analogue radiometric quantity, radiance, to obtain the amount of light across all wavelengths, and thus a more accurate measurement of the light intensity.

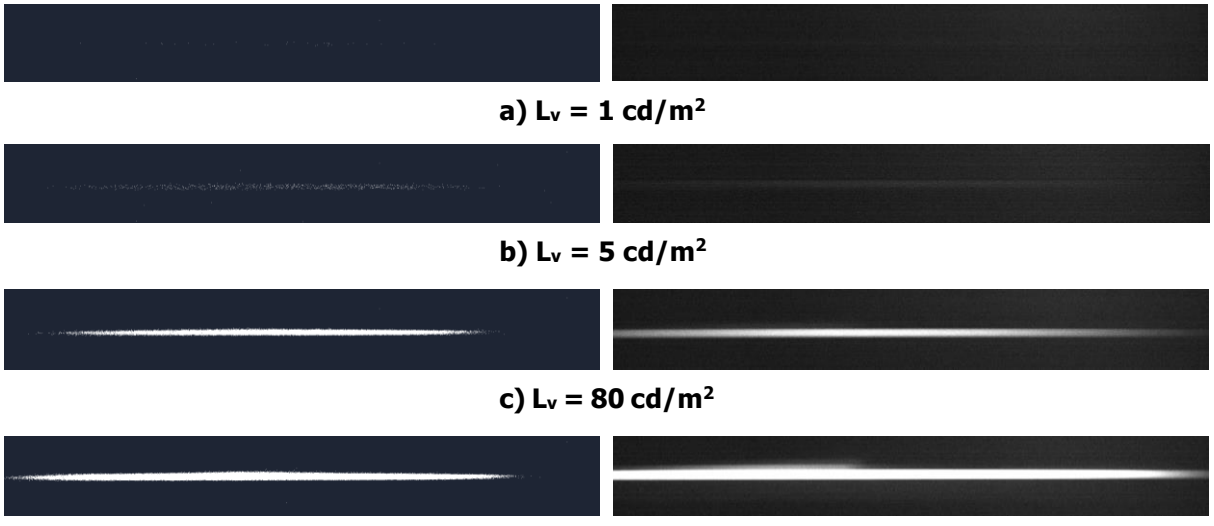

a) L_v = 1 cd/m^2

b) L_v = 5 cd/m^2

c) L_v = 80 cd/m^2

d) L_v = 500 cd/m^2

Fig. 6 Demonstration of the dynamic range. Broadband spectrum achieved with, left: EB camera spectrometer and right: standard camera spectrometer.

5. Conclusions

The work presented here demonstrates the viability of the idea to pair EB cameras with a diffraction grating to record spectra. Measurements with this neuromorphic system were performed using a range of light sources. The results show the ability of the designed neuromorphic system to capture both broadband and line spectra. Also, these early results show improvement in performance of the EB

Copyright © 2024 by author(s)

system over the standard camera typically used in authors' work, for the conditions tested. This study is ongoing and only partial results are presented here, while the full scope will be reported in a journal publication.

Additionally, although the present context of the proposed neuromorphic spectroscopy for use in airborne observations of high-speed vehicles and re-entry objects, the potential scope goes further: this new sensor could be used in applications such as observation of commercial aircraft exhaust emissions which aligns with monitoring harmful gas emissions. The developed technology can be further used for remote optical diagnostics in future land-based, semi-autonomous vehicles for on-board sensing.

References

1. Lou, M., and Griggs, B.: NASA wants to land astronauts on Mars by 2033. CNN. https://edition.cnn.com/2019/04/03/us/nasa-mars-mission-2033-scn-trnd (2019). Accessed 20 November 2023.
2. Sopek, T., Glenn, A., Clarke, J., Di Mare, L., Collen, P., McGilvray, M.: Radiative heat transfer measurements of Titan atmospheric entry in a shock tube. Journal of Thermophysics and Heat Transfer (2024). Accepted for publication.
3. McIntyre, T. J., Khan, R., Eichmann, T. N., Upcroft, B., Buttsworth, D.: Visible and Near Infrared Spectroscopy of Hayabusa Reentry Using Semi-Autonomous Tracking. Journal of Spacecraft and Rockets, 51(1), 31-36 (2014). https://doi.org/10.2514/1.A32497
4. Afshar, S., Nicholson, A. P., van Schaik, A., Cohen, G.: Event-Based Object Detection and Tracking for Space Situational Awareness. IEEE Sensors Journal, 20(24), 15117-15132 (2020). https://doi.org/10.1109/JSEN.2020.3009687
5. Jenniskens, M., Gural, P., Dynneson, L., Grigsby, B., Newman, K., Borden, M., Koop, M., Holman, D.: CAMS: Cameras for Allsky Meteor Surveillance to establish minor meteor showers. Icarus, 216, 40–61 (2011). https://doi.org/10.1016/j.icarus.2011.08.012
6. Birch, B., Zander, F., Buttsworth, D., Noller, L., Payne, A.: Hayabusa2 Capsule Reentry: Australian Airborne Observation Emission Spectroscopy Calibration and Preliminary Analysis. AIAA SciTech Forum (2022). https://doi.org/10.2514/6.2022-2151
7. Scott, C., and Inman, J.: SCIFLI Airborne Observation of the Hayabusa2 Sample Return Capsule Re-Entry. AIAA Aviation Forum (2022). https://doi.org/10.2514/6.2022-3798
8. Gallego, G., Delbrück, T., Orchard, G., Bartolozzi, C., Taba, B., Censi, A., Leutenegger, S., Davison, A., Conradt, J., Daniilidis, K., Scaramuzza, D.: Event-Based Vision: A Survey. IEEE Transactions on Pattern Analysis and Machine Intelligence, 44(1), 154-180 (2020). https://doi.org/10.1109/TPAMI.2020.3008413
9. Cohen, G., Afshar, S., van Schaik, A., Wabnitz, A., Bessell, T., Rutten, M., Morreale, B.: Event-based Sensing for Space Situational Awareness. The Advanced Maui Optical and Space Surveillance (AMOS) Technologies Conference (2017).
10. Boahen, K.: A Burst-Mode Word-Serial Address-Event Link-I: Transmitter Design. IEEE TRANSACTIONS ON CIRCUITS AND SYSTEMS-I: REGULAR PAPERS, Vol. 51, No. 7, 2004, pp. 1269–1280. https://doi.org/10.1109/TCSI.2004.830703
11. Lichtsteiner, P., Posch, C., Delbrúck, T., "A 128x128x120 dB 15 μs Latency Asynchronous Temporal Contrast Vision Sensor," IEEE JOURNAL OF SOLID-STATE CIRCUITS: REGULAR PAPERS, Vol. 43, No. 2, 2008, pp. 1269–1280. https://doi.org/10.1109/JSSC.2007.914337.
12. Suh, Y., Choi, S., Ito, M., Kim, J., Lee, Y., Seo, J., Jung, H., Yeo, D.-H., Namgung, S., Bong, J., Kim, J. s., Park, P. K. J., Kim, J., Ryu, H., Park, Y., "A 1280x960 Dynamic Vision Sensor with a 4.95-μm Pixel Pitch and Motion Artifact Minimization," 2020 IEEE International Symposium on Circuits and Systems (ISCAS), 2020, pp. 15117–15132. https://doi.org/10.1109/ISCAS45731.2020.9180436.

Copyright © 2024 by author(s)